

ASME Journal of Engineering and Science in Medical Diagnostics and Therapy Online journal at:

https://asmedigitalcollection.asme.org/medicaldiagnostics



Is It Feasible to Reconstruct Aortic Pressure Waveform Based on a One-Dimensional Uniform Model of the Arterial Tree?

Zhili Hao

Department of Mechanical and Aerospace Engineering, Old Dominion University, Norfolk, VA 23539 e-mail: zlhao@odu.edu Based on a one-dimensional (1D) uniform model of the arterial tree, various machine-learning techniques have been explored to reconstruct aortic pressure waveform (APW) from peripheral pressure waveform (PPW). This study aims to examine the feasibility of such reconstruction. Based on a 1D uniform vibrating-string model, transfer function (TF) of PPW to APW contains four harmonics-dependent parameters: value and phase of reflection coefficient (i.e., load impedance) at periphery and transmission parameter and transmission loss in the aortaperiphery section. Pressure waveforms and blood velocity waveforms at the ascending aorta (AA), the carotid artery (CA), and the radial artery (RA) of virtual health subjects at different ages in a prevalidated database are analyzed to calculate (1) reflection coefficient at the CA and the RA as two peripheries, (2) TF for the AA-CA and AA-RA sections, and (3) transmission parameter and transmission loss in the two sections. Harmonics-dependence of the four parameters varies with aging in both sections, and arterial nonuniformity makes it unpractical to configure any mathematical model for their harmonics-dependence. Instead of fluid-loading, arterial nonuniformity greatly affects transmission loss. Compared with higher harmonics, transmission loss dramatically alters reconstructed APW. A 1D uniform model allows accurate reconstruction of APW from PPW, with a caveat that baseline values of the four parameters at different harmonics under different cardiovascular (CV) conditions need to be established a priori. Alternatively, based on the baseline values, PPW can be directly utilized for inferring CV conditions. [DOI: 10.1115/1.4062468]

Keywords: aortic pressure waveform, peripheral pressure waveform, transfer function, 1D uniform model, arterial non-uniformity, harmonics-dependence

1 Introduction

Compared with peripheral pressure waveform (PPW), aortic pressure waveform (APW) carries more physiological and pathological information for the cardiovascular (CV) system but is difficult to measure noninvasively [1-3]. Therefore, transfer function (TF) has been pursued to reconstruct APW from PPW [2–5]. Compared with arterial stiffness, three clinical indices: reflection magnitude, return time, and augmentation index (AI), derived from APW have been found to carry independent clinical values and rely on the details (i.e., morphology) on APW [6–9]. Generalized transfer function (GTF, i.e., averaged over different groups of subjects) is incapable of fully reproducing the details on APW of individuals from the measured PPW [2-5]. As such, individualized TF has been pursued for reconstructed APW with the details on the measured one. In the early days of reconstruction of APW, Hope et al. [8] pointed out that individualized TF does not permit reconstruction of APW from the measured PPW for accurate

estimation of AI, and the reconstructed APW is simply the measured PPW passing through a single mathematical transformation. It was debated [9] that an error in the phase of higher harmonics causes inaccurate estimation of AI from the reconstructed APW, which is consistent with a related finding that AI is more dependent on higher harmonics of APW [10]. Later on, Westerhof et al. [7] found that individualized TF is only slightly better than GTF for reconstruction of APW of patients at rest, but remains insufficient to fully reproduce the details of APW. Furthermore, it was found that whether individualized TF improves reconstructed APW depends on CV conditions [11], implying the variations of TF with CV conditions.

Over the past decade, advancement in machine-learning techniques has prompted significant interest in individualizing the TF [5,12–15]. The majority of the studies on individualizing the TF has based on a one-dimensional (1D) uniform lossless tube-load model [3–5], in which the tube represents the uniform aorta-periphery section (i.e., the same physical properties and geometries along its length) and the load manifests wave reflection at periphery as load impedance. Based on this tube-load model, the TF contains three parameters: transmission parameter (or pulse transit time, PTT) in the aorta-periphery section, and value and phase of reflection

Contributed by the Materials Division of ASME for publication in the JOURNAL OF ENGINEERING AND SCIENCE IN MEDICAL DIAGNOSTICS AND THERAPY. Manuscript received March 9, 2023; final manuscript received April 29, 2023; published online July 21, 2023. Assoc. Editor: Stavroula Balabani.

coefficient (i.e., load impedance) at periphery [5]. It should be noted that transmission loss is mostly neglected, since it is commonly considered to be insignificant. Individualizing the TF is about identifying the values for these three parameters. A pulse signal in the arterial tree is a collection of harmonics of the heart rate and at least the first ten harmonics are needed to accurately represent APW [16,17]. Yet, since the three parameters all vary with harmonics, they translate to a total of 30 values. Currently, various machine-learning techniques have been applied to the measured pressure waveforms at the aorta and periphery of different groups of subjects for identifying the 30 values in the TF for an individual. Du et al. [5] has recently provided a good summary of different machine-learning techniques for such efforts.

Most of these machine-learning techniques have focused on tailoring harmonics-dependence of the value and phase of load impedance, since harmonics-dependence of load impedance plays the most critical role in better matching the reconstructed APW to the measured one, compared with transmission parameter [3,5]. Different models of the load have been utilized to adjust harmonics-dependence of load impedance. For instance, a three-element Windkessel model and a four-element Windkessel model have been examined [3,5], and the same three-element Windkessel model with two sets of values for lower harmonics and higher harmonics, respectively, has also been investigated [13]. These machine-learning techniques have achieved a moderate amount of success, in the sense that, as compared with GTF, APW reconstructed from the individualized TF is closer to the measured one, but it remains insufficient to fully reproduce the details on the measured APW [5]. Yet, it is the details on APW that determines those clinical indices based on APW [6–9], and the details on APW vary with CV conditions [11].

Given all the efforts on machine-leaning techniques for reconstruction of APW with accurate details, this study aims to investigate the feasibility of such reconstruction based on a 1D uniform model of the arterial tree. Recently, the author [6] developed a 1D uniform vibrating-string model for examining wave transmission and reflection between the ascending aorta (AA) and periphery, in which load impedance is found to determine input impedance, with the latter determining wave reflection at the AA and thus the details on APW. This vibrating-string model leads to the TF from PPW to APW, which is identical to the one from the 1D uniform tube-load lossless model, except that transmission loss due to fluid-loading is also included. Similar to the tube-load model, arterial nonuniformity (i.e., axially varying physical properties and geometries in an arterial segment and branching sites in the arterial tree) is neglected [5,6]. In this study, based on this vibrating-string model, pressure waveforms and blood velocity waveforms at the AA, the CA, and the radial artery (RA) of virtual healthy subjects at different ages in a prevalidated database [18] are analyzed to calculate reflection coefficient at the CA and the RA as two peripheries in the TF for the uniform AA-CA section and the uniform AA-RA section, respectively. By substituting the corresponding APW and PPW into the TF, transmission parameter and transmission loss in the two sections are calculated. Based on the calculated results, harmonics-dependence of the four parameters at different ages and the influence of transmission loss and higher harmonics on reconstructed APW are examined. For the first time, significant influence of arterial nonuniformity on transmission loss is revealed. Arterial nonuniformity makes it unpractical to configure any mathematical model for harmonics-dependence of the four parameters. Finally, the feasibility of reconstruction of APW with the details on the measured one based on a 1D uniform model is discussed.

2 Methods

2.1 Theory

2.1.1 One-Dimensional Uniform Vibrating-String Model of the Arterial Tree. Based on the 1D pulse wave propagation theory, pulsatile pressure $\Delta p(x,t)$ at position x along the arterial tree is a collection of harmonics of the heartbeat

$$\Delta p(x,t) = \sum_{n} (A_n e^{-ik_n x} + B_n e^{ik_n x}) e^{in\omega t} \tag{1}$$

where A_n and B_n denote the forward and reflected pressure wave amplitudes of the *n*th harmonic, respectively, at the AA, with ω as the fundamental angular frequency of the heart rate (HR) and $k_n = n\omega/c_n$ being the *n*th wave number. Note that c_n is the *n*th wave velocity [6]

$$c_n = c_0 \sqrt{(1 - F_{10})} = v_n e^{i\delta_n}$$
 with $c_0 = \text{PWV} = \sqrt{\frac{Eh}{2\rho_b a}}$ (2)

where E, h, and a denote the circumferential elasticity, thickness, and inner radius of the arterial wall, respectively; and ρ_b denotes blood density. The nth phase velocity is $v_n/\cos(\delta_n)$. Equation (2) is only valid for calculating wave velocity at a position in an arterial segment and does not account for arterial nonuniformity. Note that c_0 is pulse wave velocity (PWV) commonly measured in clinical studies, and F_{10} is a fluid-loading term, which is harmonics-dependent and takes complex values

$$F_{10} = \frac{2J_1(\alpha_0)}{\alpha_0 J_0(\alpha_0)} \text{ (harmonics-dependent, complex)}$$
 (3)

where $\alpha_0^2=i^3\alpha^2$, and $\alpha=a\sqrt{\rho_bn\omega/\mu}$ is the Womersley number with μ being blood viscosity.

Pulsatile pressure causes radial displacement $\eta(x, t)$ of the arterial wall and blood velocity u(x, t) (averaged across the lumen) in blood flow [6]

$$\eta(x,t) = \frac{a^2}{Eh} \sum_{r} \left(A_n e^{-ik_n x} + B_n e^{ik_n x} \right) e^{inot} \tag{4a}$$

$$u(x,t) = \frac{1}{\rho_b} \sum_{n} \frac{1 - F_{10}}{c_n} \left(A_n e^{-ik_n x} - B_n e^{ik_n x} \right) e^{in\omega t}$$
 (4b)

Equations (1) and (4) indicate that pulsatile pressure and radial wall displacement have identical waveforms. Based on Eq. (4), pulse wave propagation in the arterial tree is governed by

$$\rho_b \pi a^2 \frac{\partial^2 \eta}{\partial t^2} = \frac{Eh\pi a}{2} (1 - F_{10}) \frac{\partial^2 \eta}{\partial x^2}$$
 (5)

The standard 1D wave equation for a vibrating string is [19]

$$\rho_L \frac{\partial^2 \eta}{\partial t^2} = T \frac{\partial^2 \eta}{\partial x^2} \quad \text{with} \quad c = \sqrt{T/\rho_L} \text{ (wave velocity)} \qquad \textbf{(6)}$$

where ρ_L and T denote linear density and tension, respectively, of the string. Comparison of Eq. (5) with (6) shows that the arterial tree can be treated as a vibrating string with its equivalent linear density and tension

$$\rho_L = \rho_b \pi a^2$$
 and $T = \frac{\pi E h}{2} a (1 - F_{10})$ (7)

While linear density does not vary with harmonics, tension is harmonics-dependent and takes complex values.

2.1.2 Reconstruction of Aortic Pressure Waveform From Peripheral Pressure Waveform. It should be pointed out that Eq. (6) is also applicable to pulsatile pressure and blood velocity. Being more aligned with transverse displacement of a vibrating string, radial wall displacement is chosen for analysis here. Since radial wall displacement and pulsatile pressure have identical waveforms, radial wall displacement waveform can represent pressure waveform. As shown in Fig. 1(a), the arterial tree from the AA to periphery can be treated as a 1D uniform vibrating-string model, with the AA at x=0 and periphery at x=L. The nth wave velocity in the uniform aorta-periphery section is defined as

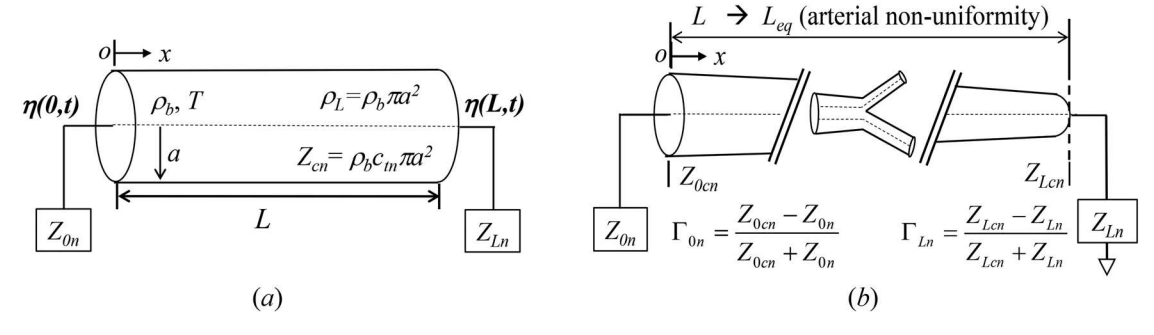


Fig. 1 Schematics of 1D pulse wave propagation in the arterial tree for wave transmission and reflection between the aorta and periphery: (a) a 1D uniform vibrating-string model (b) a 1D vibrating-string model accounting for arterial nonuniformity

$$c_{\rm tn} = v_{\rm tn} e^{i\delta_{\rm tn}} \tag{8}$$

where $v_{\rm tn}$ and $\delta_{\rm tn}$ are the value and the phase, respectively, of the *n*th wave velocity in the section, accounting for fluid loading and arterial nonuniformity. Accordingly, the *n*th phase velocity in the section is $v_{\rm tn}/\cos(\delta_{\rm tn})$. Thus, wave transmission from the AA to position *x* is characterized by transmission parameter $k_n x$ and transmission loss $\gamma_n x$ [6]

$$e^{-ik_nx}e^{-\gamma_nx}$$
 with $k_n = \frac{n\omega}{v_{\rm tn}/\cos(\delta_{\rm tn})}$ and $\gamma_n = \frac{n\omega}{v_{\rm tn}/\sin(\delta_{\rm tn})}$ (9)

Radial wall displacement at position x is given by

$$\eta_n(x,t) = (A_n e^{-ik_n x} e^{-\gamma_n x} + B_n e^{ik_n x} e^{\gamma_n x}) e^{in\omega t}$$
(10)

where A_n and B_n denote the amplitudes of the *n*th forward and reflected waves at the AA, respectively. The *n*th driving force $F_n(x,t)$ is written as

$$F_n(x,t) = -T\partial \eta_n/\partial x = \rho_L c_{\rm tn} in\omega (A_n e^{-ik_n x} e^{-\gamma_n x} - B_n e^{ik_n x} e^{\gamma_n x}) e^{in\omega t}$$
(11)

The *n*th mechanical impedance Z_n is defined as [19]

$$Z_n(x) = \frac{F_n}{\partial \eta_n / \partial t} = \rho_L c_{\text{tn}} \frac{\left(A_n e^{-ik_n x} e^{-\gamma_n x} - B_n e^{ik_n x} e^{\gamma_n x} \right)}{\left(A_n e^{-ik_n x} e^{-\gamma_n x} + B_n e^{ik_n x} e^{\gamma_n x} \right)}$$
(12)

Removing wave reflection in Eq. (12) leads to the *n*th characteristic impedance Z_{cn} [19]

$$Z_{\rm cn} = \rho_b \pi a^2 c_{\rm tn} = \rho_b \pi a^2 v_{\rm tn} e^{i\delta_{\rm tn}} \tag{13}$$

According to Eq. (10), the *n*th peripheral radial wall displacement $\eta_{pn}(t)$ becomes

$$\eta_{\rm pn}(t) = \eta_n(L, t) = (A_n e^{-ik_n L} e^{-\gamma_n L} + B_n e^{ik_n L} e^{\gamma_n L}) e^{in\omega t}$$

$$= (\eta_{\rm pfn} + \eta_{\rm pbn}) e^{in\omega t} \tag{14}$$

where $\eta_{\rm pfn}$ and $\eta_{\rm pbn}$ denote the amplitudes of the *n*th forward and reflected waves at periphery, respectively, and their ratio represents the *n*th reflection coefficient Γ_n at x=L

$$\frac{\eta_{\rm pbn}}{\eta_{\rm pfn}} = \Gamma_{\rm Ln} = \Omega_{\rm Ln} \cdot e^{i\theta_{\rm Ln}} \quad \left(\theta_{\rm Ln} < 0\right) \tag{15} \label{eq:pbn}$$

where $\Omega_{\rm Ln}$ is a real number, and $\theta_{\rm Ln} < 0$, because $\eta_{\rm pfn}$ is ahead of $\eta_{\rm pbn}$. According to Eq. (12), the *n*th load impedance $Z_{\rm Ln}$ at position x is related to $\Gamma_{\rm Ln}$ by

$$Z_{\rm Ln} = Z_{\rm Lcn} \frac{1 - \Gamma_{\rm Ln}}{1 + \Gamma_{\rm Ln}}$$
 or $\Gamma_{\rm Ln} = \frac{1 - Z_{\rm Ln}/Z_{\rm Lcn}}{1 + Z_{\rm Ln}/Z_{\rm Lcn}}$ (16)

where Z_{Lcn} denotes local characteristic impedance at periphery, which can be obtained by replacing c_{tn} with c_n in Eq. (13). As shown in Fig. 1(b), due to arterial nonuniformity, wave reflection at position x is determined by local characteristic impedance and load impedance at the position [17].

By substituting Eq. (15) into Eq. (14), the *n*th radial wall displacement $\eta_{an}(t)$ at the AA can be reconstructed from $\eta_{Dn}(t)$

$$\eta_{\rm an}(t) = (A_n + B_n)e^{in\omega t} = \frac{e^{ik_n L}e^{\gamma_n L} + \Gamma_{\rm Ln}e^{-ik_n L}e^{-\gamma_n L}}{(1 + \Gamma_{\rm Ln})}\eta_{\rm pn}(t)$$
 (17)

Reconstruction of $\eta_{an}(t)$ from $\eta_{pn}(t)$ is all about identifying the values for four parameters: transmission parameter and transmission loss in the aorta-periphery section and reflection coefficient at periphery.

2.1.3 Transmission Parameter and Transmission Loss. Arterial nonuniformity causes unknown influence on transmission parameter k_nL and transmission loss γ_nL in the aorta-periphery section. Yet, their values can be obtained from Eq. (17), if APW, PPW, and reflection coefficient at periphery are all known. The nth transfer function H_n between the AA and periphery is defined as [5,20]

$$H_n = \frac{\eta_{\rm pn}(t)}{\eta_{\rm an}(t)} = \frac{1 + \Gamma_{\rm Ln}}{e^{ik_n L} e^{\gamma_n L} + \Gamma_{\rm Ln} e^{-ik_n L} e^{-\gamma_n L}}$$
(18)

The above equation can be rewritten as a quadratic equation of $k_n L$ and $\gamma_n L$

$$(e^{ik_n L} e^{\gamma_n L})^2 - \frac{1 + \Gamma_{Ln}}{H_n} e^{ik_n L} e^{\gamma_n L} + \Gamma_{Ln} = 0$$
 (19)

Consequently, k_nL and γ_nL can be obtained from the transfer function and reflection coefficient at periphery

$$e^{ik_nL}e^{\gamma_nL} = \frac{(1+\Gamma_{\rm Ln})}{2H_n} \pm \sqrt{\left(\frac{1+\Gamma_{\rm Ln}}{2H_n}\right)^2 - \Gamma_{\rm Ln}}$$
 (20)

2.1.4 Wave Reflection at the Ascending Aorta Is Determined by Load Impedance. As shown in Eq. (17), wave reflection at the AA affects APW. Based on Eq. (12), the nth input impedance at the AA is [6]

$$Z_{0n} = Z_{0cn} \frac{A_n - B_n}{A_n + B_n} = Z_{0cn} G_n^{-1} e^{-i\phi_n} \text{ with } \frac{A_n - B_n}{A_n + B_n} = G_n^{-1} e^{-i\phi_n}$$
(21)

where $Z_{0{\rm cn}}$ denotes local characteristic impedance at the AA, as shown in Fig. 1(b), and $G_n^{-1}e^{-i\phi_n}$ is measurable at the AA and

periphery, albeit technical challenges involved in its measurement [1]. Based on Eq. (14), input impedance is related to load impedance (or reflection coefficient) at periphery by

$$Z_{0n} = Z_{0cn} \frac{A_n - B_n}{A_n + B_n} = Z_{0cn} \frac{e^{2ik_n L} e^{2\gamma_n L} - \Gamma_{Ln}}{e^{2ik_n L} e^{2\gamma_n L} + \Gamma_{Ln}}$$

$$= Z_{0cn} \frac{Z_{Lcn}(e^{2ik_n L} e^{2\gamma_n L} - 1) + Z_{Ln}(e^{2ik_n L} e^{2\gamma_n L} + 1)}{Z_{Lcn}(e^{2ik_n L} e^{2\gamma_n L} + 1) + Z_{Ln}(e^{2ik_n L} e^{2\gamma_n L} - 1)}$$
(22)

Input impedance is determined by reflection coefficient (i.e., load impedance) at periphery. This explains the reason why load impedance is so critical for reconstruction of APW [5]. Now, the question arises: based on Eq. (22), can those models for harmonic-dependent load impedance used in machine-learning techniques [3,5] translate to the true harmonics-dependent input impedance?

Other than AI, reflection magnitude and phase (i.e., return time) at the AA are two clinical indices derived from APW [1]. Reflection coefficient at the AA is related to $G_n^{-1}e^{-i\phi_n}$ by

$$\Gamma_{0n} = \frac{B_n}{A_n} = \Omega_{0n} \cdot e^{i\theta_{0n}} = \frac{G_n e^{i\phi_n} - 1}{G_n e^{i\phi_n} + 1} \quad \text{with}$$

$$\Omega_{0n} = \left| \frac{G_n e^{i\phi_n} - 1}{G_n e^{i\phi_n} + 1} \right| \quad \text{and} \quad \theta_{0n} = -a \tan \frac{2G_n \sin \phi_n}{G_n^2 - 1}$$
(23)

Based on the measured data $G_n^{-1}e^{-i\phi_n}$ in clinical studies [6], reflection magnitude Ω_{0n} and phase θ_{0n} vary with harmonics. Similar to AI, reflection magnitude and phase derived from APW depend on the details on APW [6].

2.2 Data-Processing Algorithms. Due to a lack of the related measured data, simulated data for virtual healthy subjects at different ages (25 year–75 year) in a prevalidated database [18] are chosen for analysis and are referred to as measured data here. Pressure waveforms and blood velocity waveforms in time domain at the AA, the CA, and the RA at different ages are analyzed. The CA and the RA are treated as two peripheries. All the calculation is conducted in MATLAB. First, fast Fourier transform (FFT) analysis is conducted on pressure waveform and blood velocity waveform at each artery for their first ten harmonics

$$\Delta p(t) = \sum_{n=1}^{10} \Delta p_n \cos(n\omega t + \alpha_n)$$
 (24a)

$$u(t) = \sum_{n=1}^{10} u_n \cos(n\omega t + \beta_n)$$
 (24b)

where Δp_n and α_n denote the amplitude and phase of the *n*th harmonic in pulsatile pressure, respectively, and u_n and β_n denote the amplitude and phase of the *n*th harmonic in blood velocity, respectively. Based on the harmonics of pressure waveforms at the three arteries, the transfer functions for the AA-CA section and the AA-RA section are calculated.

Load impedance at periphery and input impedance at the AA are both mechanical impedance. The *n*th measured load impedance at the CA and the RA, and the *n*th measured input impedance at the AA are then calculated as [6]

$$Z_{\text{Ln}} = \frac{(\rho_b c_0)^2 \pi a^2}{\frac{\Delta p_n}{u_n} e^{i(\alpha_n - \beta_n)}} \text{ (CA and RA)} \quad \text{and} \quad Z_{0n} = \frac{(\rho_b c_0)^2 \pi a^2}{\frac{\Delta p_n}{u_n} e^{i(\alpha_n - \beta_n)}} \text{ (AA)}$$

Note that c_0 and a in Eq. (25) take local values at each artery. Based on Eq. (13), local characteristic impedance at each artery is calculated. Consequently, reflection coefficient at each artery is obtained from Eq. (16). Afterwards, the transfer function for the AA-

CA section and reflection coefficient at the CA are substituted into Eq. (20). The solution with the positive value for k_nL is chosen as transmission parameter and the accompanying γ_nL is chosen as transmission loss for the AA-CA section. Similar, k_nL and γ_nL are calculated for the AA-RA section.

3 Results

3.1 Harmonics of Pressure Waveforms and Transfer **Function.** Figure 2 shows pressure waveforms and blood velocity waveforms at the three arteries at different ages, which are reconstructed from their first ten harmonics. Both waveforms vary with aging and between the arteries. Figure 3 illustrates the first ten harmonics of the pressure waveforms in Fig. 2. At all ages and the three arteries, lower harmonics is dominant relative to higher harmonics. With aging, lower harmonics become more dominant relative to higher harmonics. From the AA, the CA, to the RA, although lower harmonics become larger, they are less dominant relative to higher harmonics. Meanwhile, the phases for the first three harmonics vary moderately with aging at the three arteries. In contrast, the phases for the rest harmonics swing dramatically with harmonics. As shown in Fig. 4, the values and phases of transfer function for all the harmonics vary with aging in both sections. Noticeably, the values and phases of transfer function at all ages do not show any clear mathematical relation to harmonics.

3.2 Wave Reflection and Wave Transmission. As shown in Fig. 5, the values of input impedance and load impedance increase with aging for all the harmonics. The values and phases of input impedance and the values and phases of load impedance all vary with harmonics at different ages, but their variations with harmonics are quite different between different ages at each artery. Figure 6 shows the values and phases of local characteristic impedance at the three arteries. Note that phase of local characteristic impedance is the same as phase of wave velocity at each artery. Due to the large size of the AA, the value of local characteristic impedance at the AA does not vary with harmonics, and its phase is very small. While the values of local characteristic impedance at the CA and the RA increase with harmonics, the corresponding phases decrease with harmonics. As compared with their counterparts at the CA, the values at the RA show a larger increasing trend with harmonics and the phases at the RA are much larger than those at the CA. Reflection coefficient at each artery is plotted in Fig. 7. Similar to input impedance at the AA and load impedance at the CA and the RA, the values and phases of reflection coefficient vary with harmonics at each artery and their variation with harmonics varies with aging.

Substituting the results in Figs. 4 and 7 into Eq. (20) leads to calculation of transmission parameter and transmission loss in the AA-CA section and the AA-RA section, respectively. The calculated values of k_nL and γ_nL in the two sections account for arterial nonuniformity. As shown in Fig. 8, in the AA-CA section, k_nL varies moderately between different harmonics and between different ages, except that k_nL becomes much larger for the 9th and 10th harmonics at 25 year, 35 year, and 45 year. Yet, γ_nL varies significantly between different harmonics and between different ages. The attenuation factor e^{γ_nL} varies moderately with harmonics and with aging. In the AA-RA section, k_nL , γ_nL , and e^{γ_nL} all vary moderately with harmonics. Overall, the calculated results of e^{γ_nL} indicate that transmission loss increases with aging in both sections, with transmission loss in the AA-CA section being much lower than that in the AA-RA section.

The nth pulse transit time PTT_n from the AA to periphery is calculated as

$$PTT_n = \frac{k_n L}{n\omega}$$
 (26)

Based on Eq. (9), phase of the *n*th wave velocity in the aortaperiphery section is calculated as

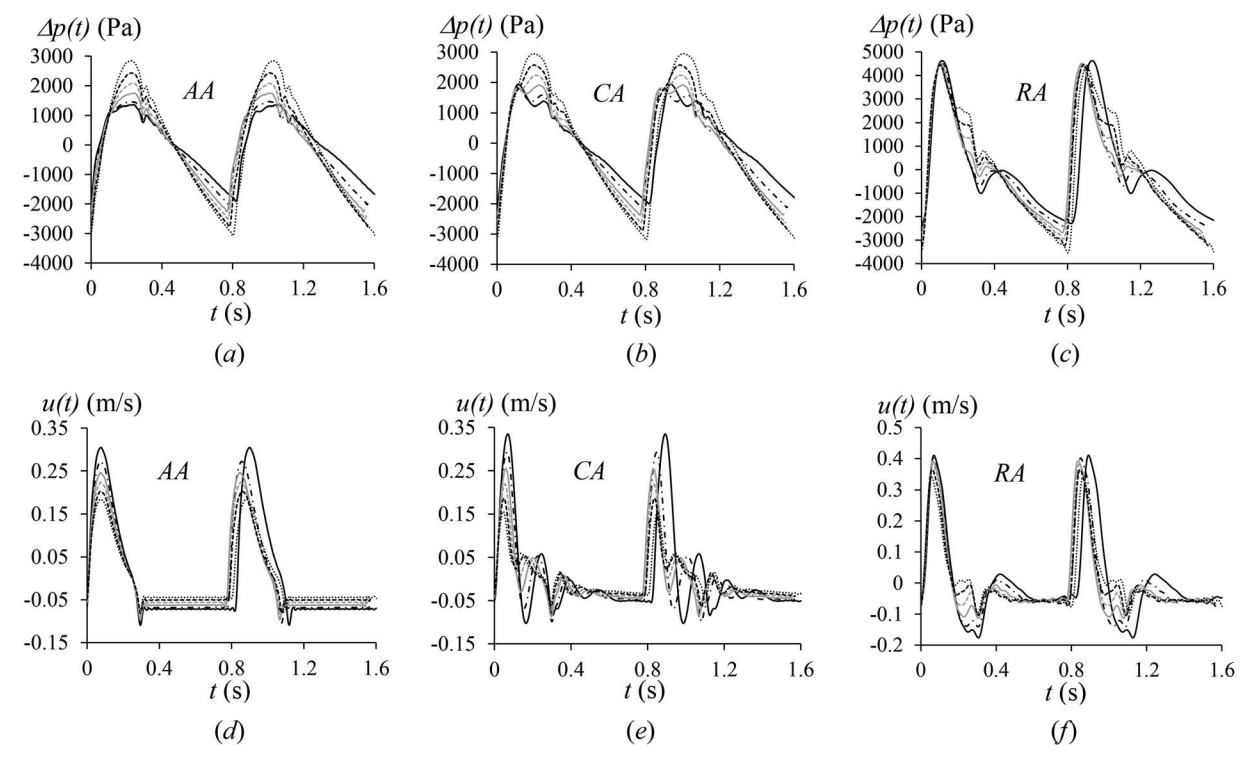


Fig. 2 Pressure waveforms and blood velocity waveforms at different ages (a) $\Delta p(t)$ (d) u(t) at the AA, (b) $\Delta p(t)$ (e) u(t) at the CA, (c) $\Delta p(t)$ (f) u(t) at the RA (25 year: — , 45 year: — , 55 year: — , 75 year: — , 75 year: — . ,

$$\delta_{\rm tn} = a \tan \left(\frac{\gamma_n L}{k_n L} \right) \qquad v_{\rm tn} = v_n \frac{\cos(\delta_{\rm tn})}{\cos(\delta_n)} \tag{28}$$

It is assumed that phase velocity $v_{\rm tn}/\cos(\delta_{\rm tn})$ in the section is equal to local phase velocity $v_n/\cos(\delta_n)$ at periphery. Then, the value of the *n*th wave velocity in the section can be obtained by

Figure 9 plots PTT_n and δ_{tn} versus harmonics in the AA-CA and AA-RA sections. In the AA-CA section, PTT shows a decreasing trend with harmonics, with PTT for the first harmonic being the

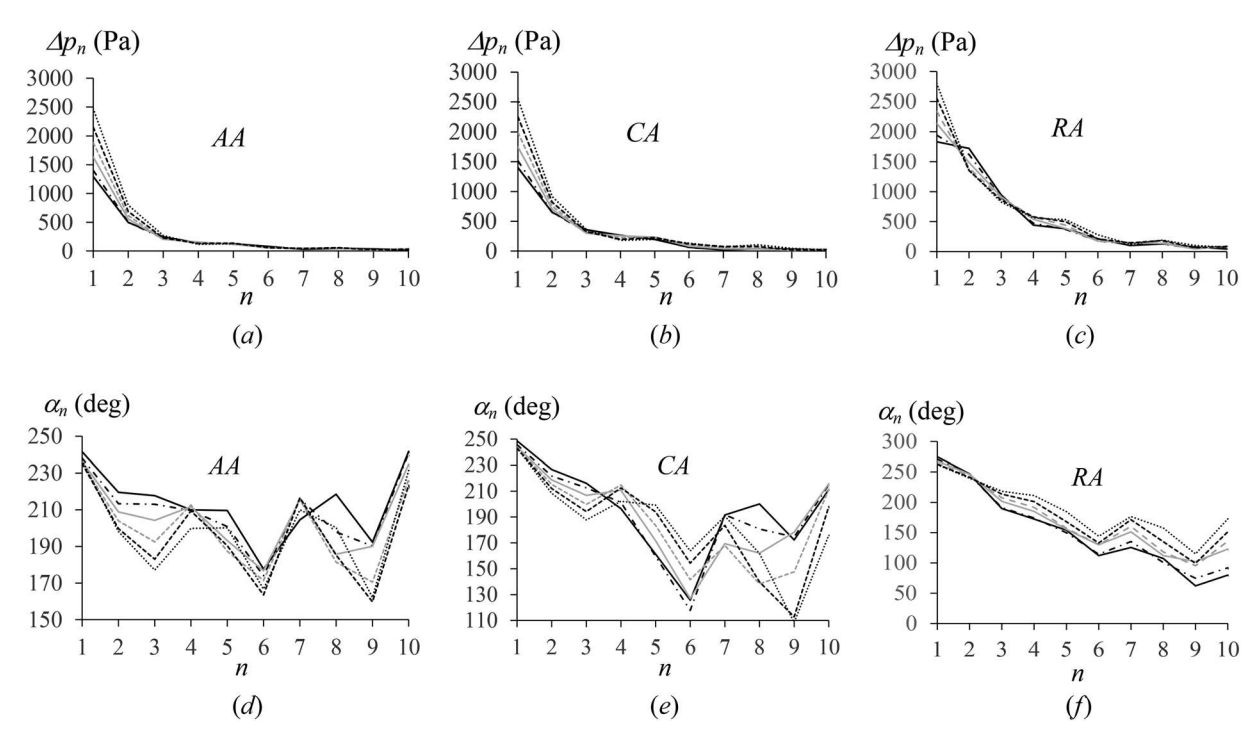


Fig. 3 First ten harmonics of pressure waveforms at different ages: (a) amplitude (d) phase at the AA, (b) amplitude (e) phase at the CA, (c) amplitude (f) phase at the RA (25 year: —, 35 year: —, 55 year: ——, 65 year: ——, 75 year: ——)

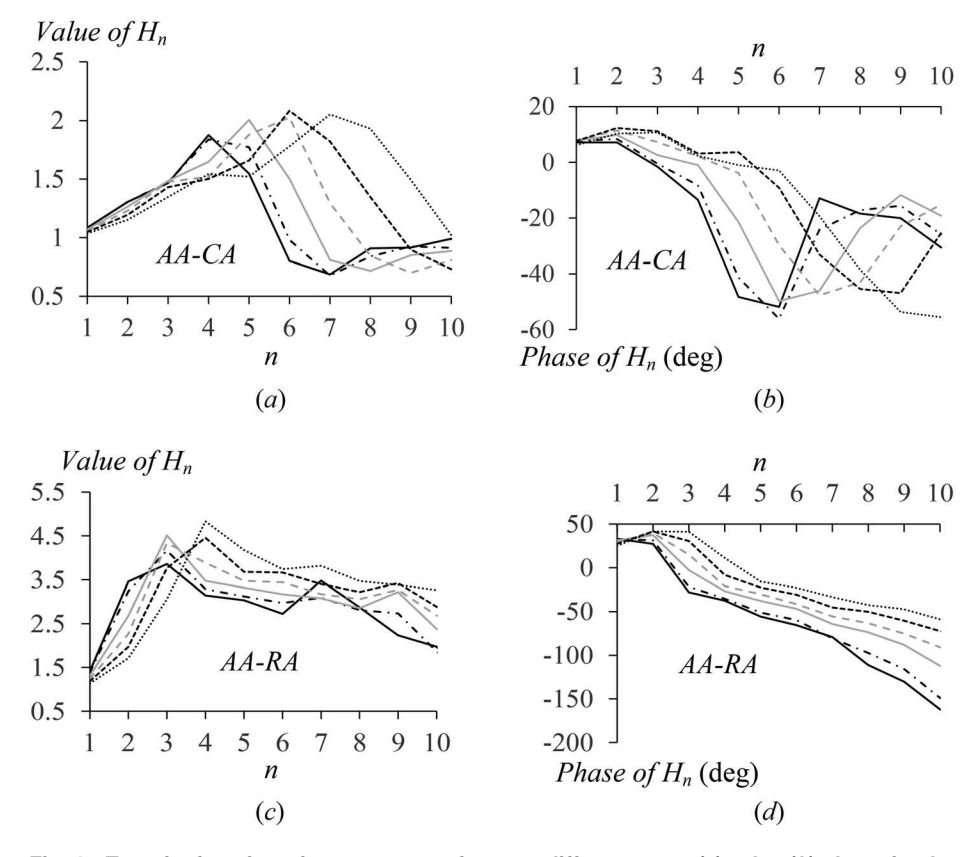


Fig. 4 Transfer function of pressure waveforms at different ages: (a) value (b) phase for the AA-CA section, (c) value (d) phase for the AA-RA section (25 year: —, 35 year: —, 45 year: —, 55 year: —--, 75 year: ——)

largest. PTT varies slightly with ages, but it does not show a clear changing trend with aging at different harmonics. Phase of wave velocity in this section varies greatly between harmonics, and shows an increasing trend with aging for the first and second harmonics. In

contrast, in the AA-RA section, PTT shows a clear decreasing trend with both harmonics and aging. Phase of wave velocity in this section shows a clear decreasing trend with harmonics and a clear increasing trend with aging. As shown in Fig. 10, the difference

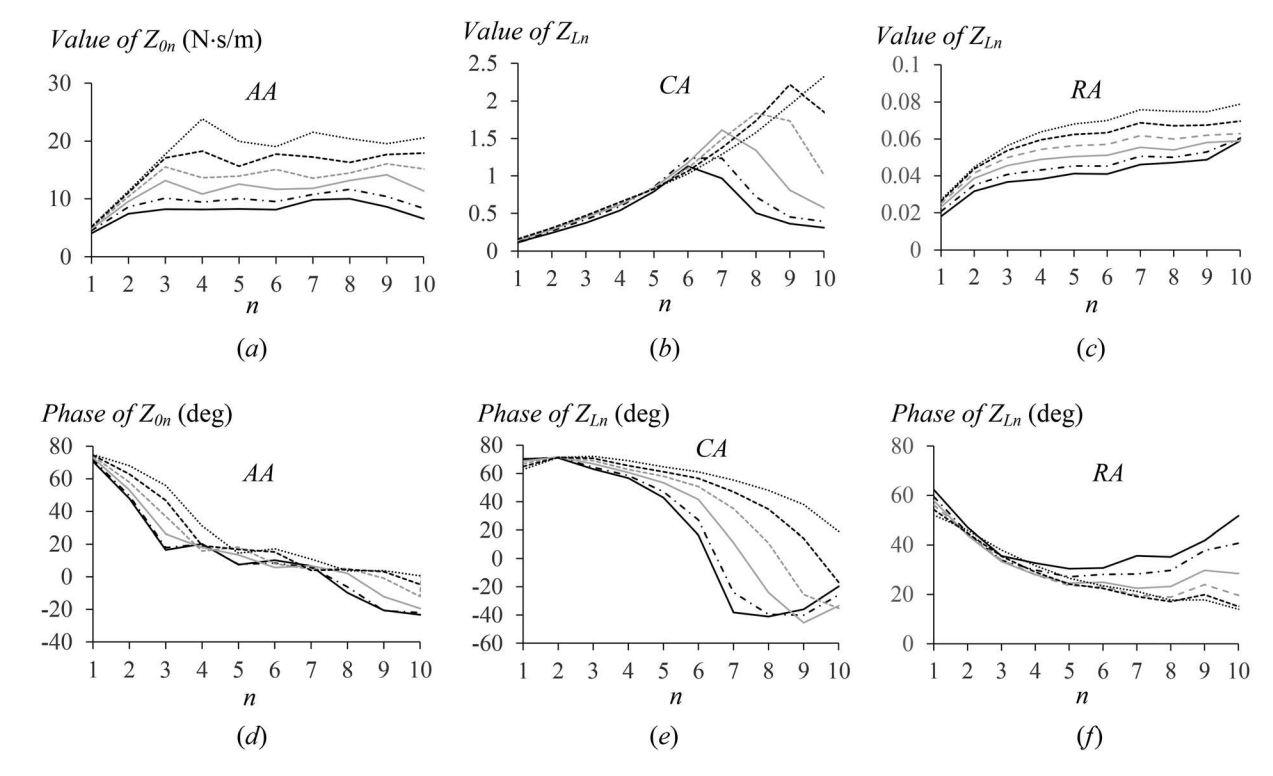


Fig. 5 Load impedance at different ages: (a) value (d) phase at the AA, (b) value (e) phase at the CA, (c) value (f) phase at the RA (25 year: —, 35 year: —, 45 year: —, 55 year: —-, 75 year: ——)

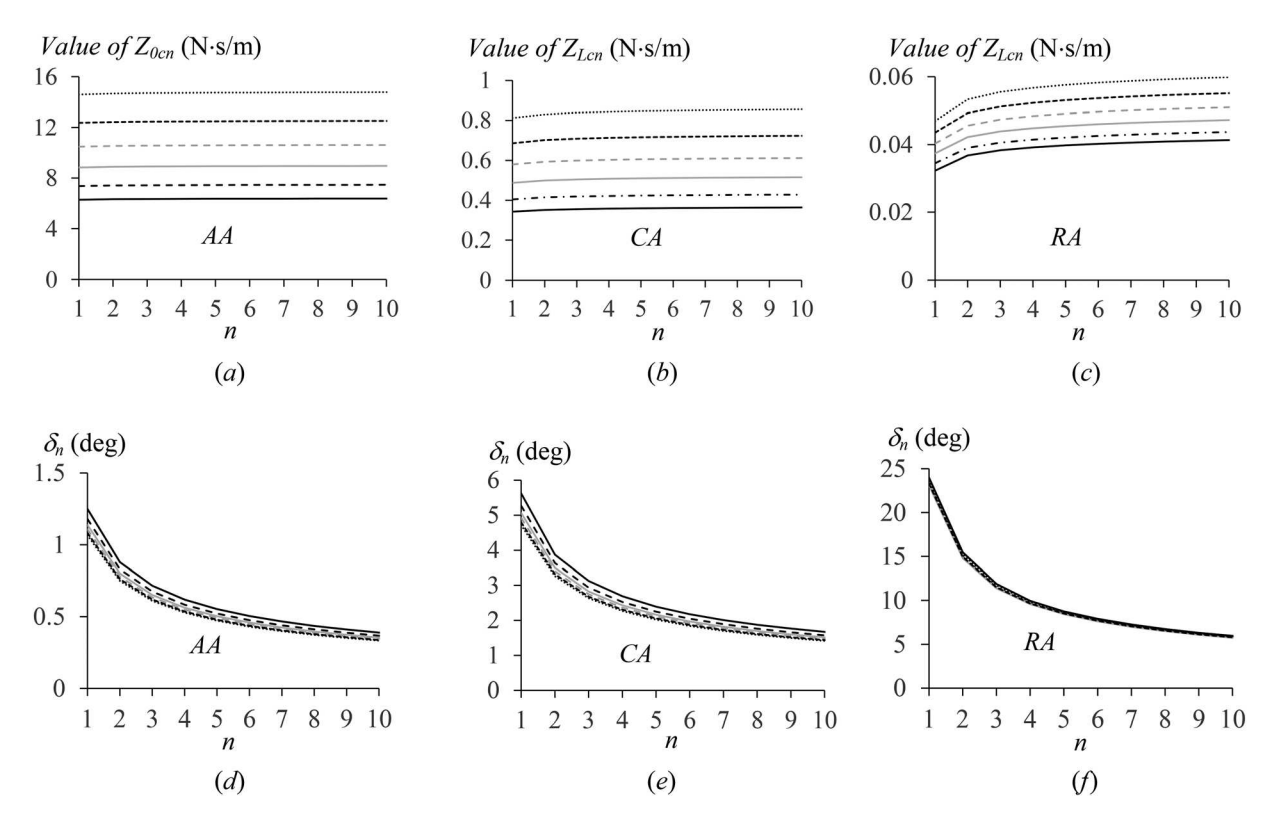
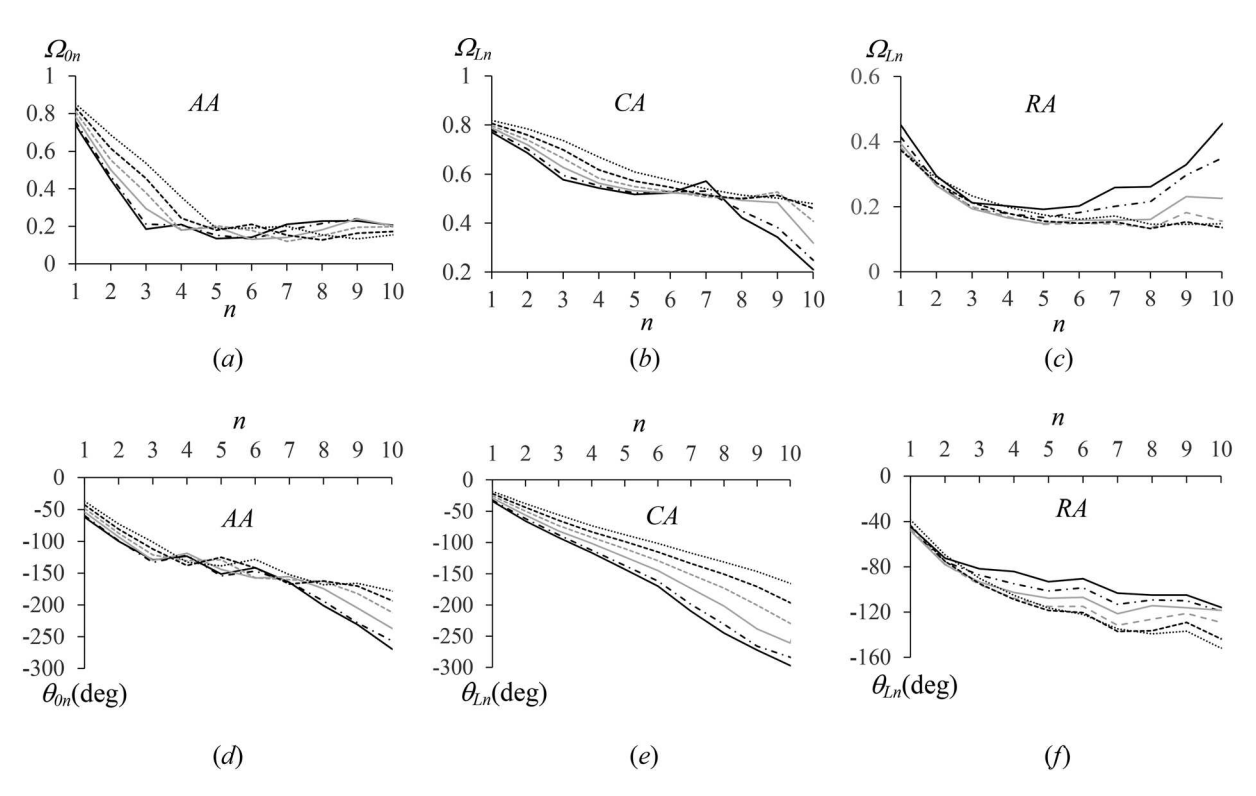


Fig. 6 Local characteristic impedance at different ages: (a) value (d) phase at the AA, (b) value (e) phase at the CA, (c) value (f) phase at the RA (25 year: —, 35 year: —, 45 year: —, 55 year: —-, 75 year: ——)



between v_m and v_n in the AA-CA section is much less than that in the AA-RA section. Comparison of δ_m in Fig. 9 with δ_n in Fig. 6 reveals that phase of wave velocity in the two sections is significantly affected by arterial nonuniformity, relative to fluid loading.

3.3 Effect of Transmission Loss and Higher Harmonics on Reconstructed Aortic Pressure Waveform. By substituting the calculated values of the parameters: $k_n L$, $\gamma_n L$, and $\Omega_{\rm Ln} \cdot e^{i\theta_{\rm Ln}}$ in Figs. 7 and 8 into Eq. (17), the reconstructed APW with the first ten

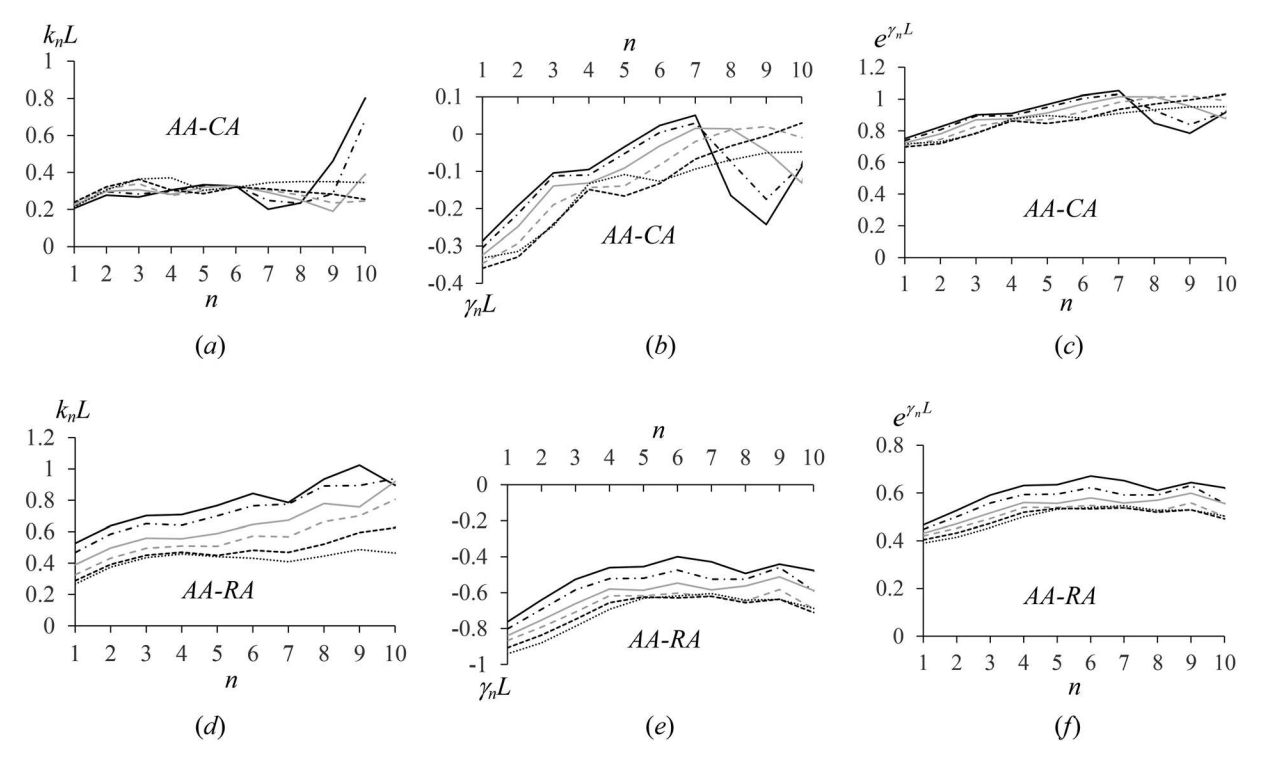


Fig. 8 Wave transmission at different ages: (a) $k_n L$ (b) $\gamma_n L$ (c) $e^{\gamma_n L}$ in the AA-CA section, (d) $k_n L$ (e) $\gamma_n L$ (f) $e^{\gamma_n L}$ in the AA-RA section (25 year: —, 35 year: —, 45 year: —, 55 year: —-, 75 year: ——)

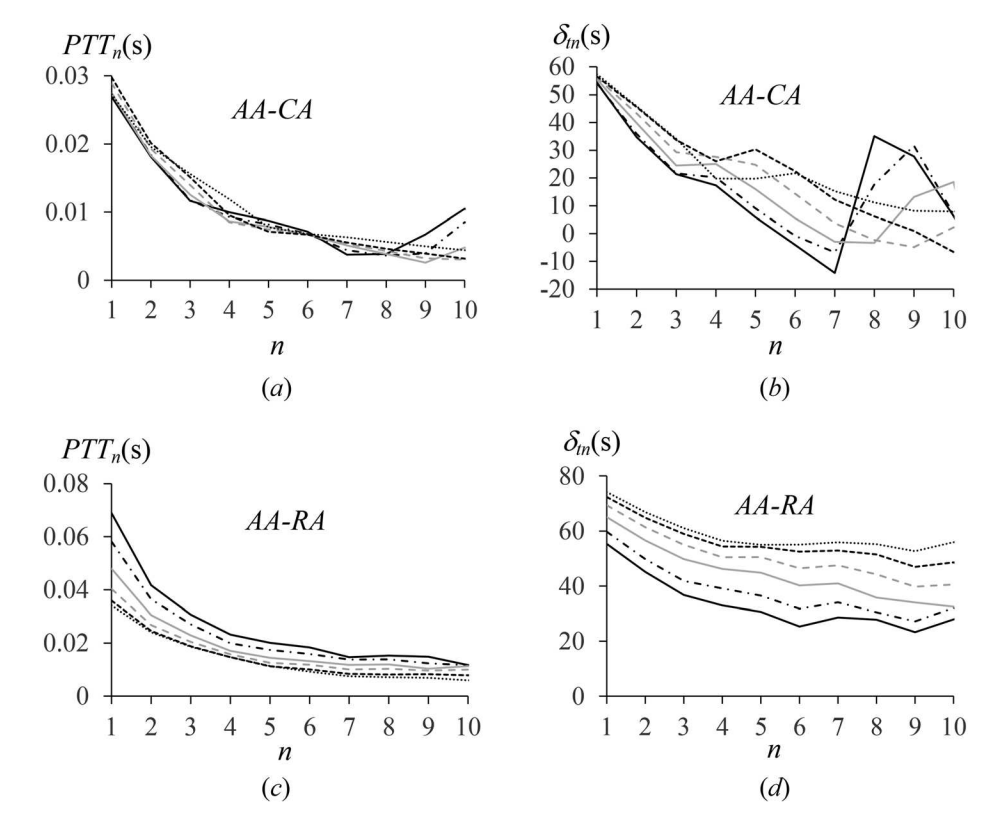


Fig. 9 PTT and phase of wave velocity at different ages: (a) PTT_n(b) δ_{tn} in the AA-CA section, (c) PTT_n(d) δ_{tn} in the AA-RA section (25 year: —, 35 year: —, 45 year: —, 55 year: —-, 55 year: —-, 75 year: …..)

harmonics for two ages: 25 year and 75 year, is plotted in Fig. 11. The reconstructed APW from the AA-CA and AA-RA sections at both ages is identical to the original APW. At both ages, while transmission loss moderately affects the reconstructed APW from

the AA-CA section, it significantly alters the reconstructed APW from the AA-RA section. In Fig. 12, only the first five harmonics are utilized to reconstruct APW. Evidently, the reconstructed APW with the first five harmonics from both sections is sufficient to accurately

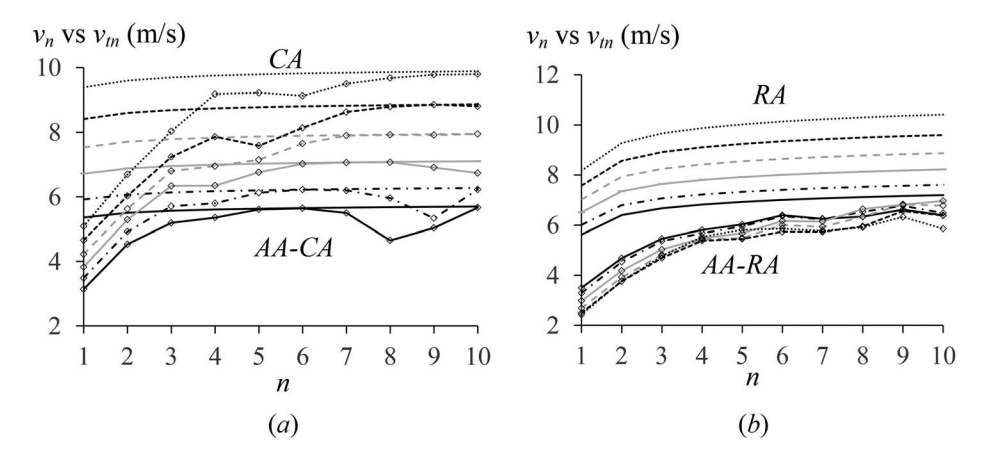


Fig. 10 Value of local wave velocity at periphery and value of wave velocity in the aortaperiphery section at different ages: (a) CA versus AA-CA section (b) RA versus AA-RA section (marker: AA-CA section and AA-RA section, no marker: CA and RA; 25 year: —, 35 year: —, 45 year: —, 55 year: —--, 75 year: …)

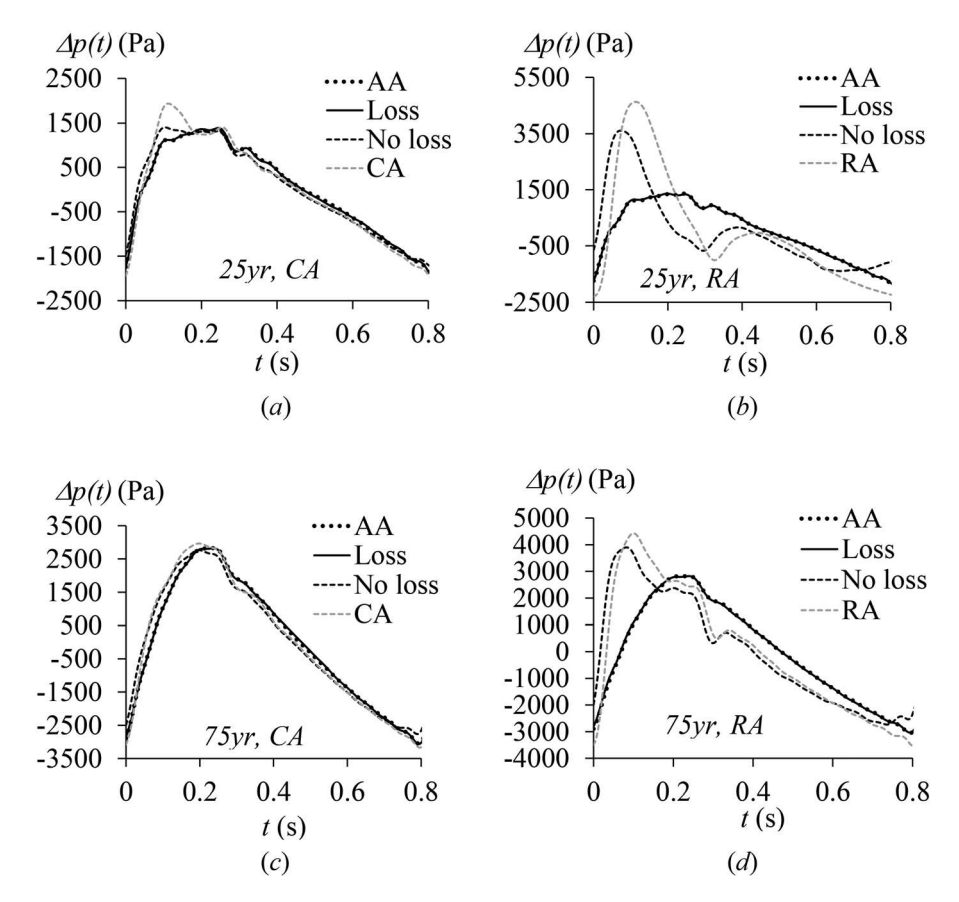


Fig. 11 Effect of transmission loss on reconstructed APW with the first ten harmonics (a) AA-CA section (b) AA-RA section for 25 year-olds, (c) AA-CA section (d) AA-RA section for 75 year-olds (Note: AA: original APW, Loss: reconstructed APW with transmission loss, No loss: reconstructed APW with no transmission loss. CA: PPW at the CA; RA: PPW at the RA.)

trace the amplitude of APW and closely match the original APW, but is insufficient to fully reproduce the details on the original APW. Interestingly, rather than higher harmonics, it is transmission loss for the first five harmonics that causes significant difference between the reconstructed APW and the original one at both ages. The fifth—tenth harmonics have less influence on accuracy of reconstructed APW at old age than at young age, because of the first to fifth harmonics being more dominant at old age. Since observations on the reconstructed APW for the other ages are the same as these two ages, their reconstructed APW are omitted.

4 Discussion

The pressure waveforms and blood velocity waveforms analyzed here were simulated from a 1D distributed model of a hierarchical branching arterial network that consists of 116 arterial segments with linearly tapered diameter and their branching sites [18]. These simulated waveforms were validated by comparing with corresponding in vivo data and well-reproduced age-related changes in hemodynamic parameters [18]. As such, these waveforms encompass the influence of arterial nonuniformity on wave transmission

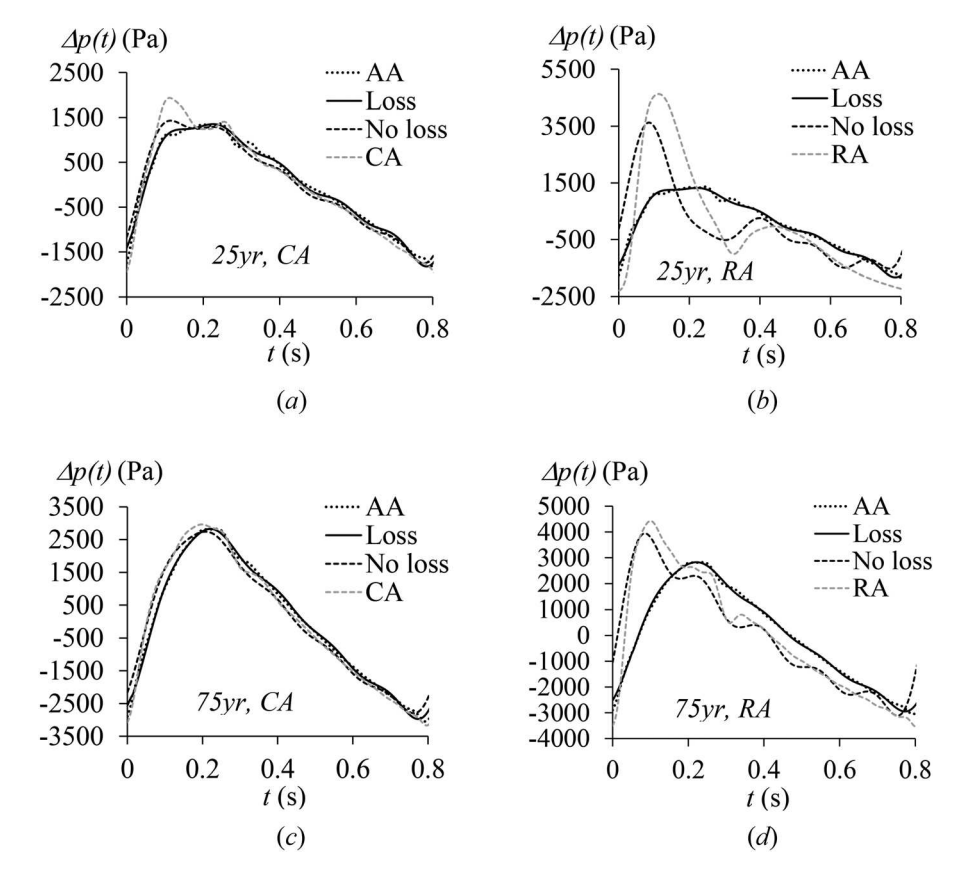


Fig. 12 Effect of transmission loss on reconstructed aortic pressure waveform with the first five harmonics (a) AA-CA section (b) AA-RA section for 25 year-olds, (c) AA-CA section (d) AA-RA section for 75 year-olds (Note: AA: original APW, Loss: reconstructed APW with transmission loss, No loss: reconstructed APW with no transmission loss. CA: PPW at the CA; RA: PPW at the RA.)

Table 1 Physical properties and geometries and the first local wave velocity at the AA, the CA, and the RA at different ages, together with the first wave velocity in the AA-CA and AA-RA sections

Age (year)		25	35	45	55	65	75
HR (bpm)		72.82	76.73	77.72	77.32	76.53	74.44
AA	$a \text{ (mm)}$ $Eh \text{ (N/m)}$ $PWV \text{ (m/s)}$ $v_1/\cos(\delta_1) \text{ (m/s)}$ $\delta_1 \text{ (deg)}$	18.36 1305.70 5.69 5.57 1.25	18.94 1629.00 6.26 6.13 1.18	19.50 2148.40 7.08 6.94 1.14	20.06 2770.40 7.93 7.78 1.11	20.64 3538.90 8.83 8.67 1.08	21.23 4523.70 9.85 9.67 1.07
CA	a (mm) Eh (N/m) PWV (m/s) δ_I (deg) v_I /cos(δ_I) (m/s)	4.37 329.67 5.86 5.63 5.38	4.52 411.52 6.44 5.27 5.94	4.66 543.47 7.29 5.07 6.74	4.80 700.51 8.15 4.92 7.56	4.94 896.00 9.09 4.80 8.44	5.08 1146.78 10.13 4.72 9.42
AA-CA	v_{tI} (m/s) δ_{tI} (deg)	3.14 54.34	3.49 54.08	3.83 55.44	4.22 56.05	4.66 56.52	5.09 57.32
RA	a (mm) Eh (N/m) PWV (m/s) δ_I (deg) v_I /cos(δ_I) (m/s)	1.31 180.12 7.91 23.98 6.15	1.31 200.37 8.34 23.28 6.54	1.31 233.70 9.01 23.11 7.08	1.31 272.53 9.73 23.18 7.64	1.31 319.12 10.53 23.31 8.25	1.31 376.69 11.44 23.68 8.93
AA-RA	v_{tI} (m/s) δ_{tI} (deg)	3.50 55.36	3.29 59.78	2.98 65.09	2.69 69.40	2.49 72.41	2.43 74.22

Table 2 Influence of arterial nonuniformity on wave transmission for the first harmonic: (a) AA-CA section (b) AA-RA section

(a) AA-CA section										
Age (year)	25	35	45	55	65	75				
L(m)	0.188	0.189	0.19	0.19	0.191	0.192				
$PTT_{I}(s)$	0.0269	0.0275	0.0275	0.0289	0.0298	0.0273				
L/PTT_I (m/s)	6.98	6.88	6.92	6.57	6.41	7.03				
$L_{\mathrm{eq}I}$ (m)	0.1450	0.1633	0.1852	0.2186	0.2514	0.2574				
$k_I L$ (no unit)	0.2058	0.2206	0.2234	0.2334	0.2380	0.2129				
$\gamma_I L$ (no unit)	-0.2870	-0.3047	-0.3244	-0.3470	-0.3600	-0.3321				
$e^{\gamma_1 L}$ (no unit)	0.7505	0.7373	0.7230	0.7068	0.6977	0.7174				
(b) AA-RA section										
Age (year)	25	35	45	55	65	75				
L(m)	0.785	0.785	0.785	0.785	0.785	0.785				
$PTT_{I}(s)$	0.0689	0.0582	0.0480	0.0404	0.0360	0.0341				
L/PTT_I (m/s)	11.39	13.49	16.37	19.45	21.82	23.00				
$L_{\text{eq}l}$ (m)	0.4240	0.3806	0.3395	0.3082	0.2968	0.3046				
$k_I L$ (no unit)	0.5267	0.4673	0.3902	0.3258	0.2874	0.2658				
$\gamma_I L$ (no unit)	-0.7628	-0.8027	-0.8405	-0.8674	-0.9069	-0.9415				
$e^{\gamma_1 L}$ (no unit)	0.4663	0.4481	0.4315	0.4201	0.4038	0.3900				

and wave reflection in the arterial tree. Consequently, the above-calculated results based on a 1D uniform model are believed to account for arterial nonuniformity.

4.1 Influence of Arterial Non-Uniformity on Wave Transmission. Table 1 summarizes physical properties and geometries [18] and the first phase velocity and δ_I at the three arteries. For comparison, the values of δ_{tI} and v_{tI} in the AA-CA and AA-RA sections are also listed. While δ_I is solely from fluid-loading, δ_{tI} accounts for both fluid-loading and arterial nonuniformity in each section. Despite the large variation of a and Eh between the three arteries, PWV is similar at the AA and the CA at the same age. In contrast, PWV at the RA is noticeably larger than its counterparts at the AA and the CA. Interestingly, when fluid-loading is accounted for, phase velocity becomes quite similar at the three arteries at the same age. Arising solely from fluid loading, δ_I increases from the AA, the CA to the RA, because fluid loading becomes more pronounced at small arteries.

Table 2 summarizes the influence of arterial nonuniformity on wave transmission for the first harmonic in the AA-CA and the AA-RA sections. While PTT_I decreases with aging until 65 year in the AA-CA section, it decreases with aging from 25 year to 75 year in the AA-RA section. The physical length L of the AA-CA and the AA-RA sections is obtained from the arterial geometrical network used in the database [18]. Based on this physical length, phase velocity calculated as L/PTT_I does not show a changing trend with aging in the AA-CA section. Although phase velocity in the AA-RA section show a clear increasing trend with aging, its value is well above local phase velocity at the AA and the RA in Table 1. As such, an equivalent transmission length $L_{\rm eq1}$ for the first harmonic is defined as

$$L_{\text{eq}1} = \text{PTT}_1 \cdot v_1 / \cos(\delta_1) \tag{29}$$

where the first local phase velocity $v_I/\cos(\delta_I)$ at the CA and the RA is utilized for the AA-CA and AA-RA sections, respectively. It is worth mentioning that this local phase velocity increases with aging at each artery and is similar between the three arteries. While $L_{\rm eq1}$ for the AA-CA section is close to its physical length and increases with aging, $L_{\rm eq1}$ for the AA-RA section is well below its physical length and decreases with aging. As shown in Table 1, v_{tI} in the two sections follows the same changing trend with aging as $L_{\rm eq1}$ in their respective sections.

Comparison of δ_{tn} in the two sections in Fig. 9 with δ_n at the CA and the AA in Fig. 6 reveals that arterial nonuniformity significantly alters transmission loss in both sections, as compared with fluid-

loading. Moreover, the influence of arterial nonuniformity on transmission loss varies with harmonics. As shown in Table 2, the attenuation factor $e^{\gamma_1 L}$ in both sections shows a decreasing trend with aging. Given the dominant influence of arterial nonuniformity on transmission loss, it might be concluded that transmission loss caused by arterial nonuniformity varies with aging.

Taken together, arterial nonuniformity alters the equivalent transmission length and causes significant harmonics-dependent transmission loss, relative to fluid-loading. The influence of arterial nonuniformity on transmission parameter and transmission loss is not only harmonics-dependent, but also varies with aging. In other words, when physical properties and geometries in the three arteries vary with aging, so does the influence of arterial nonuniformity on transmission parameter and transmission loss. It is worth mentioning that, by analyzing the influence of wave reflection on APW along the aorta length, a clinical study also revealed harmonics-dependent wave transmission [21].

To improve reconstructed APW based on the uniform tube-load model, an exponentially tapered tube-load model was proposed to account for arterial nonuniformity [15]. Yet, it was found that the obtained values are not physiologically consistent with the aortic tapering, and the improvement on reconstructed APW is only marginal, as compared with the uniform tube-load model. While an exponentially tapered tube may account for the tapered geometry in an arterial segment, but it does not account for multiple branching sites from the aorta to periphery. As shown here, the influence of arterial nonuniformity on transmission parameter is significant, in terms of altering the equivalent transmission path. Efforts were also taken to add transmission loss to the tube-load model for improving reconstructed APW [22]. It was found that the lossy tube-load model in general outperforms the lossless tube-load model. Yet, transmission loss and transmission parameter in the model were related by a simple mathematical relation, which was derived from characteristic impedance and load impedance without considering arterial nonuniformity. As shown in Fig. 8, it does not seem like that influence of arterial nonuniformity on transmission parameter and transmission loss can be related by a simple mathematical model.

4.2 Influence of Arterial Non-Uniformity on Wave Reflection at Periphery. Given the observed wave reflection at periphery, the arterial tree has a finite length and thus a termination. Then, load impedance at the two arteries is affected by termination impedance [6]. It has been well established that a tapered geometry causes harmonics-dependent boundary conditions, leading to harmonics-dependence of termination impedance [19]. However, due to mathematical complexity, a mathematical relation of termination

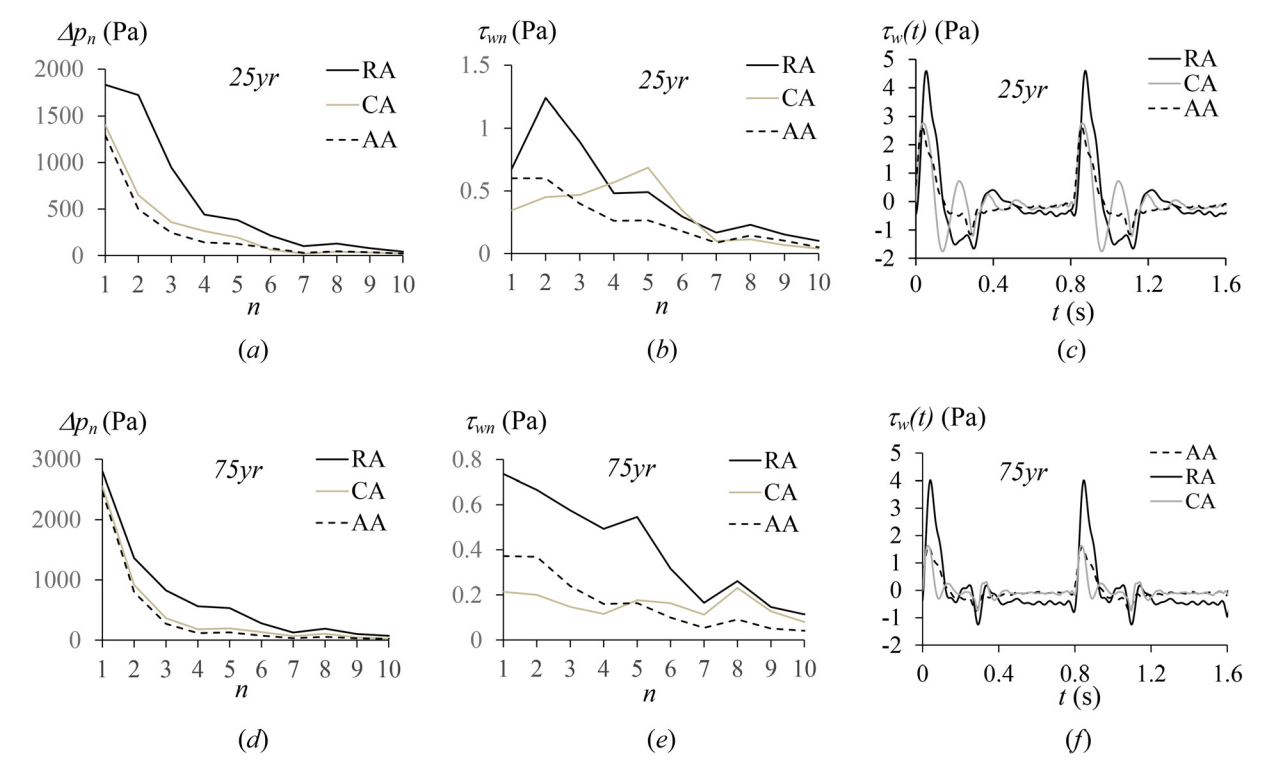
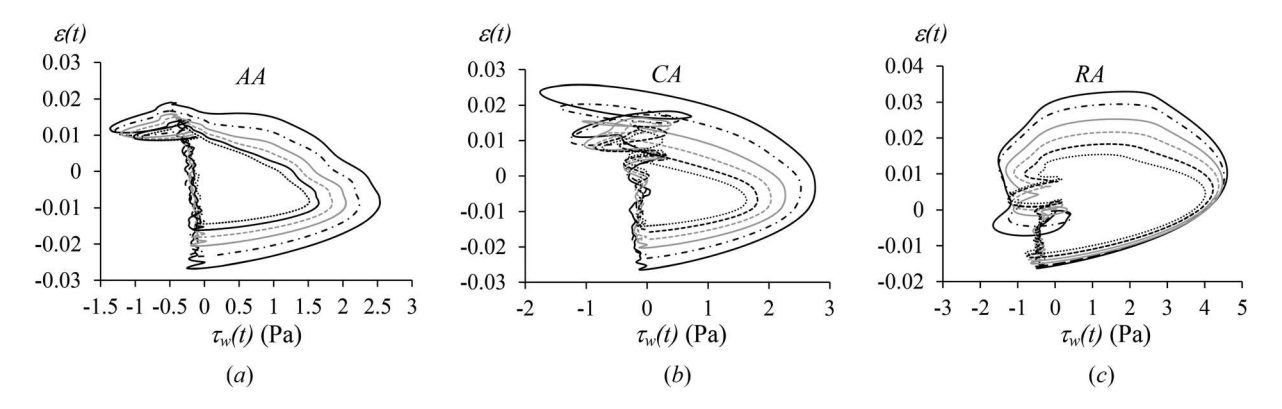


Fig. 13 First ten harmonics of pressure waveforms, first ten harmonics of WSS waveforms, and WSS waveforms at the AA, the CA, and the RA (a) Δp_n (b) τ_{wn} (c) τ_w (t) for 25 year-olds, (d) Δp_n , (e) τ_{wn} , and (f) τ_w (t) for 75 year-olds



impedance to harmonics does not exist [19]. Arterial nonuniformity further alters the relation of termination impedance to harmonics, making harmonics-dependence of termination impedance theoretically unpredictable. Consequently, it is unpractical, if not impossible, to configure any mathematical model for harmonics-dependence of load impedance. This explains why all the Windkessel models in various forms are incapable of capturing the true harmonics-dependence of load impedance for reconstructing APW with the details on the measured one [3,5].

4.3 Influence of Branching Sites on Endothelial Function. The arterial tree contains a hierarchical branching arterial network. When pressure waves move from large arteries to small arteries, they need to pass through multiple branching sites. The obtained values of transmission parameter and transmission loss in the AA-CA and the AA-RA sections account for branching sites. As shown in Fig. 13, there is significant difference in harmonics of pressure waveform between the three arteries. Since tapered geometry of an arterial segment is not expected to cause such difference, it might be

inferred that branching sites are behind rearrangement of harmonics of pressure waveform at different arteries, through mode-coupling (energy transfer between different harmonics). Difference in harmonics of pressure waveform between the three arteries leads to their difference in harmonics of wall shear stress (WSS) and WSS waveform $\tau_w(t)$, as shown in Fig. 13.

Endothelial cells (EC) lining the inner surface of the arterial wall play a critical role in vascular growth, remodeling, and homeostasis [23]. EC are exposed to WSS, and are sensitive to both WSS amplitude and waveform (or harmonics of WSS) [23,24]. Changes in WSS amplitude and waveform are thought to undermine regulation behavior of EC and ultimately lead to endothelial dysfunction, which precedes arterial stiffening [23]. As such, WSS amplitude and waveform have been utilized as an indicator of endothelial function. Besides WSS, EC are exposed to circumferential strain (CS) $\varepsilon(t) = \eta(t)/a$ in the arterial wall. Synergistic effects of WSS and CS on endothelial function were also reported [25].

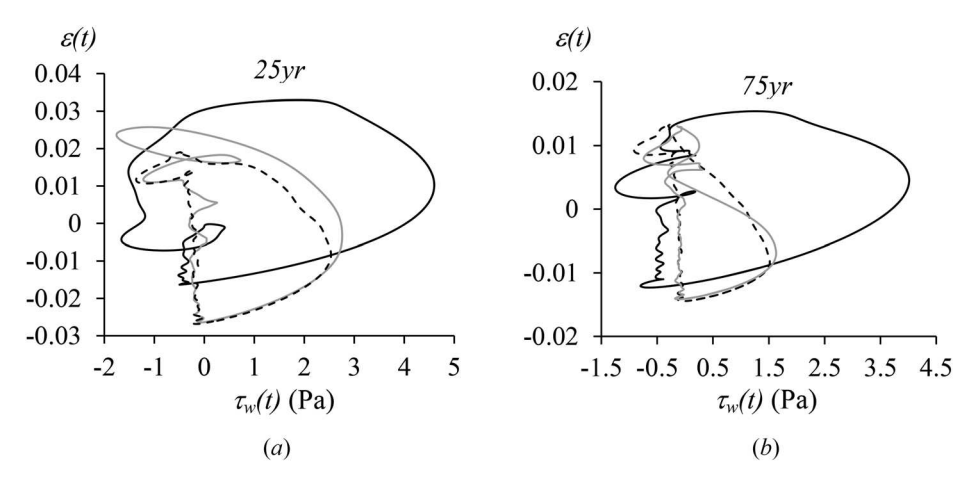


Fig. 15 WSS-CS loop (or $\tau_w(t) \sim \varepsilon(t)$ loop) at the AA, the CA and the RA (a) for 25 year-olds (b) for 75 year-olds (AA: ---, CA: —, RA: —)

Based on the calculated values in Sec. 3, WSS-CS loops at the three arteries are plotted in Fig. 14. Although the shape of WSS-CS loop at each artery does not vary with aging, its size decreases with aging. Given that these WSS-CS loops are from healthy subjects, it might be concluded that the shape of WSS-CS loop is more important to endothelial function, relative to its size. The shape of WSS-CS loop varies between the three arteries. As shown in Fig. 15, as the artery size decreases, the size and length of WSS-CS loop increase. Given that physiological function of an artery is to deliver nutrients and oxygen to the body, small arteries might demand an increased size and length of WSS-CS loop for achieving its physiological function. As such, by rearranging harmonics of pressure waveform from large arteries to small arteries, branching sites facilitate endothelial function in arteries of different sizes.

4.4 Feasibility of a One-Dimensional Uniform Model for Reconstruction of Aortic Pressure Waveform From Peripheral Pressure Waveform. Despite its dramatic physical and geometrical complexity, the arterial tree has been treated as a 1D uniform model, which is widely used in understanding CV physiology and interpreting measured arterial pulse signals for CV disease detection. As the gold standard for assessment of global arterial stiffness in clinical studies, carotid-femoral pulse wave velocity (cfPWV) is based on the 1D uniform model and its clinical values have been well established [1].

As shown in Sec. 3, a 1D uniform model of the arterial tree allows reconstruction of APW to PPW with exactly the same details on the original APW. However, the values of the four parameters involved in such reconstruction must account for physiological realities. First, transmission loss significantly alters the reconstructed APW and must be included in reconstruction of APW. Second, arterial nonuniformity causes extremely complicated harmonicsdependence of the four parameters, which can not be captured by rather simplified mathematical relations, such as those used in the tube-load model [5,21]. The variation of harmonics-dependence of the four parameters with CV conditions further exacerbates the efforts on identifying such mathematical relations. As such, although it is feasible to reconstruct APW from PPW based on a 1D uniform model, the baseline values of the four parameters at different harmonics under different CV conditions must be established a priori. Since establishing the baseline values allows relating clinical values of APW to PPW, PPW might be directly utilized for inferring CV conditions.

4.5 Study Limitations. Although the values of the four parameters at different harmonics in reconstruction of APW from PPW at different ages are obtained here, they are calculated from the simulated data on virtual healthy subjects. Then, accuracy of the

obtained results depends on accuracy of the simulated data. Although the simulated data was validated by corresponding in vivo data and age-related changes in hemodynamic parameters [18], they may not be identical to the measured data, given individual variations. It is expected that the values of the four parameters and their harmonics-dependence might be different from the actual measured data on healthy subjects at different ages. Nevertheless, the findings on the influence of arterial nonuniformity on wave transmission and wave reflection at different ages are expected to remain valid. In addition, only the effect of aging on harmonics-dependence of the four parameters is considered. It is expected that harmonics-dependence of the four parameters varies with CV conditions [11], similar to the effect of CV conditions on harmonics of PPW [26-28]. Finally, it is worth noting that fluid loading in Eq. (3) results from a rather simplified blood velocity profile in an artery [29,30]. Given their geometrical complexity, fluid loading at branching sites is expected to greatly differ from Eq. (3). Complex fluid flow is believed to contribute to modecoupling and transmission loss happening at branching sites.

5 Conclusion

By applying a 1D uniform vibrating-string model of the arterial tree to analyze pressure waveforms and blood velocity waveforms at the AA, the CA and the RA of virtual health subjects at different ages in a prevalidated database, the feasibility of reconstruction of APW from PPW based on a 1D uniform model is validated. As compared with fluid-loading, arterial nonuniformity is found to dramatically affect transmission loss, which further greatly alters the reconstructed APW. Arterial nonuniformity causes complicated harmonics-dependence of the four parameters involved in reconstruction of APW. As such, baseline values of the four parameters at different harmonics under different CV conditions need to be established a priori. Alternatively, based on the baseline values, PPW can be directly utilized for inferring CV conditions.

References

- Mynard, J. P., Kondiboyina, A., Kowalski, R., Cheung, M. M. H., and Smolich, J. J., 2020, "Measurement, Analysis and Interpretation of Pressure/Flow Waves in Blood Vessels," Front. Physiol., 11, p. 1085.
- [2] Westerhof, B. E., and Westerhof, N., 2012, "Magnitude and Return Time of the Reflected Wave: The Effects of Large Artery Stiffness and Aortic Geometry," J. Hypertens., 30(5), pp. 932–939.
- [3] Zhang, G., Hahn, J. O., and Mukkamala, R., 2011, "Tube-Load Model Parameter Estimation for Monitoring Arterial Hemodynamics," Front. Physiol., 2, p. 72.
- [4] Zhou, S., Xu, L., Hao, L., Xiao, H., Yao, Y., Qi, L., and Yao, Y., 2019, "A Review on Low-Dimensional Physics-Based Models of Systemic Arteries: Application to Estimation of Central Aortic Pressure," Biomed. Eng. Online, 18(1), p. 41.
- [5] Du, S., Yao, Y., Sun, G., Wang, L., Alastruey, J., Avolio, A. P., and Xu, L., 2023, "Personalized Aortic Pressure Waveform Estimation From Brachial Pressure Waveform Using an Adaptive Transfer Function," Comput. Biol. Med., 155, p. 106654.

- [6] Hao, Z., 2023, "A Vibrating-String Model for Closed-Loop Wave Transmission and Reflection Between the Aorta and Periphery," ASME J. Med. Diagn., 6(4), p. 041001.
- [7] Westerhof, B. E., Guelen, I., Stok, W. J., Lasance, H. A., Ascoop, C. A., Wesseling, K. H., Westerhof, N., Bos, W. J., Stergiopulos, N., and Spaan, J. A., 2008, "Individualization of Transfer Function in Estimation of Central Aortic Pressure From the Peripheral Pulse is Not Required in Patients at Rest," J. Appl. Physiol., 105(6), pp. 1858–1863.
- [8] Hope, S. A., Meredith, I. T., and Cameron, J. D., 2008, "Arterial Transfer Functions and the Reconstruction of Central Aortic Waveforms: Myths, Controversies and Misconceptions," J. Hypertens., 26(1), pp. 4–7.
- [9] O'Rourke, M. F., and Adji, A., 2012, "Noninvasive Studies of Central Aortic Pressure," Curr. Hypertens. Rep., 14(1), pp. 8–20.
- [10] Chen, C. H., Nevo, E., Fetics, B., Pak, P. H., Yin, F. C., Maughan, W. L., and Kass, D. A., 1997, "Estimation of Central Aortic Pressure Waveform by Mathematical Transformation of Radial Tonometry Pressure: Validation of Generalized Transfer Function," Circulation, 95(7), pp. 1827–1836.
- [11] Stok, W. J., Westerhof, B. E., Guelen, I., and Karemaker, J. M., 2011, "Aortic Pressure Wave Reconstruction During Exercise is Improved by Adaptive Filtering: A Pilot Study," Med. Biol. Eng. Comput., 49(8), pp. 909–916.
- [12] Gao, M., Rose, W. C., Fetics, B., Kass, D. A., Chen, C. H., and Mukkamala, R., 2016, "A Simple Adaptive Transfer Function for Deriving the Central Blood Pressure Waveform From a Radial Blood Pressure Waveform," Sci. Rep., 6(1), p. 33230.
- [13] Du, S., Liu, W., Yao, Y., Sun, G., He, Y., Alastruey, J., Xu, L., Yao, Y., and Qian, W., 2022, "Reconstruction of the Aortic Pressure Waveform Using a Two-Level Adaptive Transfer Function Strategy," Measurement, 204, p. 112111.
- [14] Hao, L., Zhang, Q., Liu, J., Wang, Z., Xu, L., and van de Vosse, F. N., 2022, "A Strategy to Personalize a 1D Pulse Wave Propagation Model for Estimating Subject-Specific Central Aortic Pressure Waveform," Comput. Biol. Med., 146, p. 105528.
- [15] Mousavi, A., Tivay, A., Finegan, B., McMurtry, M. S., Mukkamala, R., and Hahn, J. O., 2019, "Tapered vs. Uniform Tube-Load Modeling of Blood Pressure Wave Propagation in Human Aorta," Front. Physiol., 10, p. 974.
- [16] Qureshi, M. U., Colebank, M. J., Schreier, D. A., Tabima, D. M., Haider, M. A., Chesler, N. C., and Olufsen, M. S., 2018, "Characteristic Impedance: Frequency or Time Domain Approach?," Physiol. Meas., 39(1), p. 014004.
- [17] Westerhof, B. E., and Westerhof, N., 2018, "Uniform Tube Models With Single Reflection Site Do Not Explain Aortic Wave Travel and Pressure Wave Shape," Physiol. Meas., 39(12), p. 124006.

- [18] Charlton, P. H., Mariscal, H. J., Vennin, S., Li, Y., Chowienczyk, P., and Alastruey, J., 2019, "Modelling Arterial Pulse Waves in Healthy Ageing: A Database for in Silico Evaluation of Haemodynamics and Pulse Wave Indices," Am. J. Physiol. Heart Circ. Physiol., 317(5), pp. H1062–H1085.
- [19] Kinsler, L. E., Frey, A. R., Coppens, A. B., and Sanders, J. V., 2000, Fundamentals of Acoustics, 4th ed., Wiley Inc., Hoboken, NJ.
- [20] Westerhof, B. E., van Gemert, M. J. C., and van den Wijngaard, J. P., 2020, "Pressure and Flow Relations in the Systemic Arterial Tree Throughout Development From Newborn to Adult," Front. Pediatr., 8, p. 251.
- [21] Hope, S. A., Tay, D. B., Meredith, I. T., and Cameron, J. D., 2005, "Waveform Dispersion, Not Reflection, May Be the Major Determinant of Aortic Pressure Wave Morphology," Am. J. Physiol. Heart Circ. Physiol., 289(6), pp. H2497–H2502.
- [22] Abdollahzade, M., Kim, C. S., Fazeli, N., Finegan, B. A., Sean McMurtry, M., and Hahn, J. O., 2014, "Data-Driven Lossy Tube-Load Modeling of Arterial Tree: In-Human Study," ASME J. Biomech. Eng., 136(10), p. 101011.
- [23] Baeyens, N., Bandyopadhyay, C., Coon, B. G., Yun, S., and Schwartz, M. A., 2016, "Endothelial Fluid Shear Stress Sensing in Vascular Health and Disease," J. Clin. Invest., 126(3), pp. 821–828.
- [24] Feaver, R. E., Gelfand, B. D., and Blackman, B. R., 2013, "Human Haemodynamic Frequency Harmonics Regulate the Inflammatory Phenotype of Vascular Endothelial Cells," Nat. Commun., 4(1), p. 1525.
- Vascular Endothelial Cells," Nat. Commun., 4(1), p. 1525.

 [25] Zhao, S., Suciu, A., Ziegler, T., Moore, J. E., Bürki, E., Meister, J.-J., and Brunner, H. R., 1995, "Synergistic Effects of Fluid Shear Stress and Cyclic Circumferential Stretch on Vascular Endothelial Cell Morphology and Cytoskeleton," Arterioscler., Thromb., Vasc. Biol., 15(10), pp. 1781–1786.
- cler., Thromb., Vasc. Biol., 15(10), pp. 1781–1786.
 [26] Chang, C. W., Liao, K. M., Chang, Y. T., Wang, S. H., Chen, Y. C., and Wang, G. C., 2019, "Fourth Harmonic of Radial Pulse Wave Predicts Adverse Cardiac Events in Asymptomatic Patients With Type 2 Diabetes," J. Diabetes Complications, 33(6), pp. 413–416.
- [27] Hsiu, H., Liu, J. C., Yang, C. J., Chen, H. S., Wu, M. S., Hao, W. R., Lee, K. Y., Hu, C. J., Wang, Y. H., and Fang, Y. A., 2022, "Discrimination of Vascular Aging Using the Arterial Pulse Spectrum and Machine-Learning Analysis," Microvasc. Res., 139, p. 104240.
- [28] Chen, P.-J., Wu, H.-K., Hsu, P.-C., Lo, L.-C., Chang, H.-H., and Worsnop, C., 2020, "Effects of Five Daily Activities on Harmonic Analysis of the Radial Pulse," J. Evidenced-Based Complementary Altern. Med., 2020, pp. 1–5.
- [29] Painter, P. R., 2008, "The Velocity of the Arterial Pulse Wave: A Viscous-Fluid Shock Wave in an Elastic Tube," Theor. Biol. Med. Modell., 5(1), p. 15.
- [30] San, O., and Staples, A. E., 2012, "An Improved Model for Reduced-Order Physiological Fluid Flows," J. Mech. Med. Biol., 12(03), p. 1250052.